Water-Soluble Hybrid Nanoclusters with Extra Bright and Photostable Emissions: A New Tool for Biological Imaging

Natallia Makarava,* Alexander Parfenov,* and Ilia V. Baskakov*[†]

*Medical Biotechnology Center, University of Maryland Biotechnology Institute, Baltimore, Maryland 21201;
and [†]Department of Biochemistry and Molecular Biology, University of Maryland School of Medicine, Baltimore, Maryland 21201

ABSTRACT   We report the generation of a previously unknown class of water-soluble organic-inorganic hybrid nanoclusters composed of silver and thioflavin T with remarkable fluorescent properties. These hybrid nanoclusters display an extra bright fluorescence in aqueous solutions without any detectable photobleaching. Furthermore, the fluorescent nanoclusters can be generated in situ by sensitized photoreduction of Ag^+. Organic-inorganic nanoclusters have remarkable advantages over the known classes of fluorescent probes for the development of ultrasensitive biological assays, cell imaging, or studies of single molecules. As an example of a practical biological application, imaging of amyloid fibrils produced from recombinant mammalian prion proteins and nonprion proteins using hybrid nanoclusters is presented.

INTRODUCTION

Photoactive nanocomposites of noble metals are of great interest in various fields of physics and chemistry (1). Generation of noble luminescent nanoclusters has been mostly confined to the gaseous and solid phase and does not occur in aqueous solutions at ambient temperatures (2,3). Thus, their practical application in biology has been limited. To date, two procedures for generating fluorescent nanoclusters of noble metals by encapsulating silver nanodots into dendrimers or into oligonucleotides have been reported (4,5). In this study, we developed an alternative procedure for generating silver nanoclusters using sensitized photoreduction of Ag^+ in aqueous solution at room temperature. Our approach resulted in the formation of water-soluble fluorescent nanoclusters composed of silver and organic fluorophore thioflavin T (ThT). These hybrid nanoclusters displayed ultrabright fluorescence in aqueous solution without any detectable photobleaching. The hybrid nanoclusters have remarkable advantages over the known classes of fluorescent probes for studies of single molecules, cell imaging, and the development of ultrasensitive biological assays. As an example of a practical biological application, imaging of amyloid fibrils produced from prion protein and insulin using hybrid nanoclusters is presented.

MATERIALS AND METHODS

Reagents

ThT was purchased from Sigma (St. Louis, MO); silver nitrate (99+%) was from Aldrich (Milwaukee, WI). Recombinant human prion protein encompassing residues 90–231 and full length mouse prion protein composed of residues 23–231 were expressed in *Escherichia coli* and purified and refolded in vitro into amyloid fibrils as previously described (6,7).

Fluorescence was recorded on a FluoroMax-3 fluorimeter (Jobin Yvon-Spex, Edison, NJ) in 1.0-cm rectangular cuvettes with excitation at 330 nm (an excitation slit of 3 nm and an emission slit of 3 nm) in photon counting mode.

Epifluorescence microscopy was carried out on an inverted microscope (Nikon (Melville, NY) Eclipse TE2000-U) with an illumination system X-Cite 120 (EXFO Photonics Solutions, Mississauga, Canada) connected through fiber optics using a 1.3 aperture Plan Fluor 100× NA objective. The emission was isolated from Rayleigh- and Raman-shifted light by a combination of filters: an excitation filter 485DF22, a beam splitter 505DRLPO2, and an emission filter 510LP (Omega Optical, Brattleboro, VT). Digital images were acquired using a cooled 12-bit CoolSnap HQ CCD camera (Photometrics, Tucson, AZ). The emission spectra were collected on an Ocean Optics (Dunedin, FL) S2000 spectrofluorimeter coupled to the fluorescent microscope through fiber optics.

Dynamic light scattering

Dynamic light scattering experiments were conducted using a DynaPro model MSX (Protein Solutions, Charlottesville, VA) equipped with an 824 nm laser. The stock solution of ThT was mixed with $AgNO_3$ solutions, centrifuged to remove dust and aggregated particles, and photoactivated, as described above. Supernatant solution (25 μL) was transferred to a standard quartz cuvette, and the scattered light was measured at 22°C at the angle of 90° to the incident beam. After accumulation of at least 30 data points, the experimental data were analyzed using the Dynamics version 6.3 software package supplied by the manufacturer (Protein Solutions). Briefly, the hydrodynamic radius (R_h) was calculated from the diffusion coefficient using the Stokes-Einstein equation.

Electron microscopy

The samples were adsorbed for 30 s to carbon-coated 100-mesh grids, washed with 0.1 M and 0.01 M Na-acetate for 5 s each, dried, and then viewed in a Zeiss (Oberkocken, Germany) EM 10 CA electron microscope.

Formation of the amyloid fibrils

To form amyloid fibrils from prion proteins, a stock solution of rPrP (3 mg/ml) in 6 M GdnHCl was diluted to a final protein concentration of 0.5 mg/ml

and incubated at 37°C for 48 h in 1 M GdnHCl, 3 M urea, 150 mM NaCl at pH 5.5 in 20 mM Na-acetate buffer with continuous shaking at 600 RPM using a Delfia plate shaker (Wallac, Boston, MA) in conical plastic tubes (Eppendorf, Westbury, NY) in a reaction volume >0.4 ml. The kinetics of fibril formation was monitored using a ThT-binding assay as described previously (6). Amyloid fibrils were dialyzed against 10 mM Na-acetate buffer (pH 5.5) overnight and diluted into 10 mM Na-acetate buffer (pH 5.5) to a final concentration of rPrP of 1 μM; ThT and AgNO$_3$ were then added and illuminated at room temperature as specified.

To form amyloid fibrils from insulin, an aqueous solution of bovine insulin (Sigma) was prepared at a concentration of 1 mM; the pH was then adjusted to 2.0 with HCl and followed by overnight incubation at 65°C as described previously (8). Fibrils formed from chicken egg white lysozyme (Sigma) were prepared by incubation of 1 mM protein in aqueous solution at pH 2.0 (pH was adjusted using HCl) for 5 days at 65°C as described previously (9). The kinetics of fibrils formation by insulin and lysozyme was monitored using the ThT-binding assay.

Generation of hybrid nanoclusters in situ

Amyloid fibrils of rPrP (1 μM) or insulin (1 μM) were incubated with ThT (10 μM) for 3 min at room temperature in 10 mM Na-acetate buffer (pH 5.5); AgNO$_3$ was then added to a final concentration as specified. Solution (10 μl) was placed on a coverslip and illuminated at 475 nm with an irradiance of ~500 W/cm^2 as specified.

Laser scanning confocal microscopy was carried out on the LSM 510 Axioskop System (Zeiss) using a 1.3 aperture Zeiss C-Apochromat 40× oil objective and krypton/argon laser at 458 nm. Dual images of ThT-Ag clusters were simultaneously acquired by two photomultipliers using a dichroic mirror and bandpass filter to separate the emission of ThT at 510 nm from the silver reflectance at 458nm.

RESULTS

Previous studies demonstrated that UV irradiation of Ag$^+$ in aqueous solutions results in reduction of Ag$^+$ to atomic Ag^0 with subsequent agglomeration into Ag$_2$, Ag$_4$, and larger nanoclusters (10,11). We found that Ag clusters that produce bright and photostable fluorescence can be generated in aqueous solutions of AgNO$_3$ (10 μM) upon prolonged irradiation either with UV or visible light up to 500 nm (Fig. 1 a). However, the low efficiency of direct photoinduced generation of fluorescent silver clusters forced us to look for other alternatives. Because formation of colloidal silver was recently achieved by sensitized photoreduction of Ag$^+$ in aqueous solution (12), we sought to explore whether a similar approach could be used for a more efficient generation of fluorescent silver clusters.

We found that the addition of AgNO$_3$ (0.1 μM) to an aqueous solution of organic fluorophore ThT (10 μM) at room temperature at first quenched ThT fluorescence by 50% (Fig. 2 a). As many heavy cations are known to quench fluorescence (13), formation of weak coordination complexes of Ag$^+$ with the sulfur atom of the ThT benzothiazole ring may account for this initial quenching (14). Surprisingly, upon subsequent brief illumination of the ThT (10 μM)/ AgNO$_3$ (0.1 μM) solutions at 312 nm, we observed a notable growth of fluorescence intensity (Fig. 2 b). The fluorescence intensity continued to increase each time upon repetitive
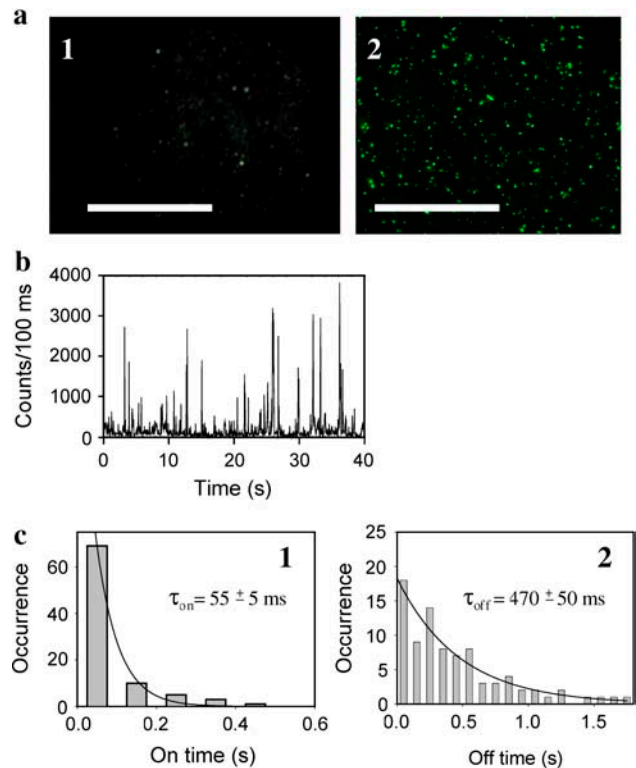

FIGURE 1 Epifluorescence microscopy images of silver nanoclusters induced by irradiation at 475 nm. (a) Microscopy images of Ag nanoclusters (*panel 1*) and hybrid Ag-ThT nanoclusters (*panel 2*), scale bar = 10 μm. Ag clusters appeared in a field of view upon illumination of aqueous 10 μM AgNO$_3$ for 1 h, whereas hybrid Ag-ThT clusters appeared upon illumination of aqueous ThT (10 μM)/AgNO$_3$ (1 μM) after only 3 min. Drops of AgNO$_3$ or ThT/AgNO$_3$ solutions (50 μl) were placed on coverslips and illuminated at 475 nm (irradiance 500 W/cm^2) at room temperature. Exposure time for collecting the image was 0.2 s. (b) Fluorescent blinking observed from a randomly selected single Ag-ThT nanocluster. Emission was acquired for 400 frames with 100-ms time resolution for each frame. Fluorescence was recorded with an irradiance of 500 W/cm^2 using a metal halide lamp (Hamamatsu, Bridgewater, NJ). (c) Histograms of on- and off-times (*panels 1* and *2*, respectively) of the data shown in b. The histograms are calculated using a threshold intensity of 300 counts/100 ms. The monoexponential decay (*solid lines*) gives an apparent $\tau_{on} = 55 \pm 5$ and $\tau_{off} = 470 \pm 50$ ms for this excitation irradiance.

cycles of illumination of ThT/AgNO$_3$ solution at 312 nm with a mercury lamp (approximate irradiance of 0.1 W/cm^2; Fig. 2 b). While doing these experiments, we noticed that fluorescence enhancement could be achieved even without external illumination of the ThT/AgNO$_3$ solution by using only the excitation beam of the fluorescence spectrometer during fluorescence measurement (λ_{ex} = 330 nm; 330 nm corresponds to the excitation maximum of ThT when it is used in the absence of amyloid fibrils; Fig. 2 e). Therefore, in the following experiments, we monitored the kinetics of fluorescence enhancement of ThT/AgNO$_3$ solutions illuminated directly in the chamber of the fluorescence spectrometer using an excitation beam with wavelength at 330 nm and an approximate irradiance of 1 W/cm^2 (Fig. 2 c). After only
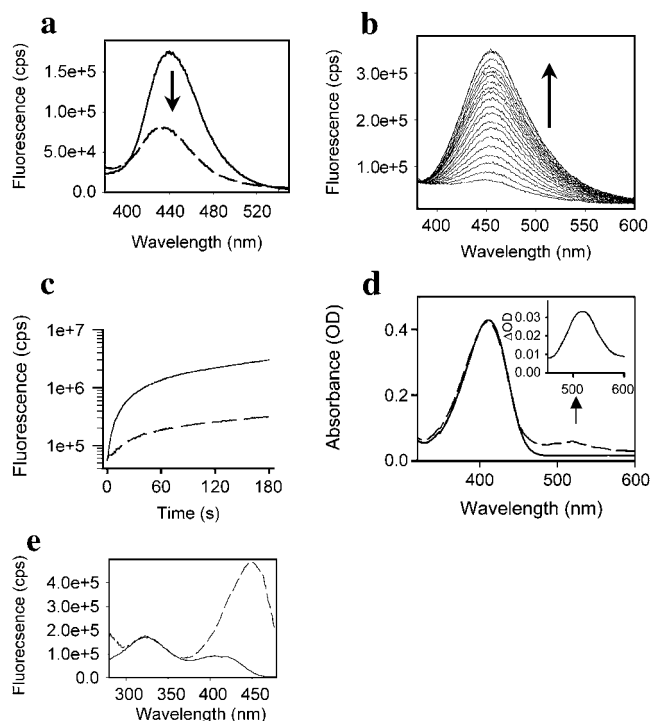
FIGURE 2 Sensitized photoreduction of Ag^+ in the presence of ThT resulted in the generation of hybrid Ag-ThT nanoclusters. (*a*) Emission spectra in aqueous solution of ThT alone (10 μM, *solid line*) and immediately after addition of $AgNO_3$ (0.1 μM, *dashed line*) collected upon excitation at 330 nm.(*b*) Emission spectra of aqueous ThT (10 μM)/ $AgNO_3$ (0.1 μM) solution recorded during repetitive cycles of illumination; the bottommost spectrum corresponds to time zero and the topmost spectrum to 180 s of illumination. Each cycle included illumination of the ThT/ $AgNO_3$ solution in a quartz cuvette (10 × 10 × 40 mm) for 10 s at 312 nm with approximate irradiance 0.1 W/cm^2 from a mercury lamp (Fotodyne, Hartland, WI), model 3-300). (*c*) Kinetics of photoreduction in aqueous solutions of ThT (10 μM)/$AgNO_3$ (0.1 μM, *dashed line*) and ThT (10 μM)/ $AgNO_3$ (10 μM, *solid line*) monitored as a change of ThT fluorescence at 450 nm upon excitation at 330 nm. Photoreduction was achieved by illumination of the cuvette directly in the chamber of a FluoroMax-3 spectrometer, under excitation wavelength at 330 nm with a slit width of 1 nm and approximate irradiance of 1 W/cm^2. ThT is known to have abnormal photophysical properties, in particular the ThT excitation maximum ($\sim$330 nm) does not correspond to the ThT absorption peak ($\sim$400 nm; (31)); therefore, in these experiments we used the excitation wavelength that corresponds to the excitation maximum of 330 nm (see *panels d* and *e*). (*d*) The absorption spectra of 10 μM ThT alone (*solid line*) and in the presence of 0.5 μM $AgNO_3$ (*dashed line*) monitored after UV illumination at 312 nm for 3 min. To correct the last spectrum for scattering, the absorption spectrum for 0.5 μM $AgNO_3$ alone was subtracted. Sensitized photoreduction was accompanied by the appearance of a peak at 520 nm (*inset*), a characteristic of silver nanoclusters (5). (*e*) The excitation spectra of 10 μM ThT alone (*solid line*) and in the presence of fibrillar rPrP, 1 μM (*dashed line*). λ_{em} = 482 nm. The spectra were corrected for scattering.

3 min of illumination, the fluorescence intensity of ThT exceeded the original level by fivefold in aqueous solutions of ThT (10 μM)/$AgNO_3$ (0.1 μM) and by $\sim$50-fold if the molar ratio of ThT to $AgNO_3$ was 1:1 (Fig. 2 *c*).

Remarkably, instead of the photobleaching that usually accompanies UV illumination of organic fluorophores, we

observed significant growth of fluorescence during sensitized photoreduction. We noticed that sensitized photoreduction of the $AgNO_3$/ThT solutions was accompanied by the appearance of a plasmon absorption peak at 520 nm—a characteristic of agglomerated Ag^0 (Fig. 2 *d*). Previous studies demonstrated that the agglomeration of noble metals into nanodots and nanocomposites is usually accompanied by the appearance of plasmon absorption, with a maximum between 380 and 600 nm, depending on the size and composition of nanocomposites (3,4,15–17). For instance, oligonucleotide-bound silver nanoclusters displayed two broad absorption peaks with maxima at 424 nm and 520 nm (5). Therefore, growth of the fluorescence emission and appearance of plasmon absorption at 520 nm was indicative of Ag^+ reduction to atomic Ag^0 and the subsequent coaggregation of Ag^0 with ThT and formation of hybrid ThT-Ag nanocomposites.

To test whether sensitized photoreduction resulted in silver agglomeration, we employed dynamic light scattering and electron microscopy. Using dynamic light scattering, we observed formation of small particles with average Stokes
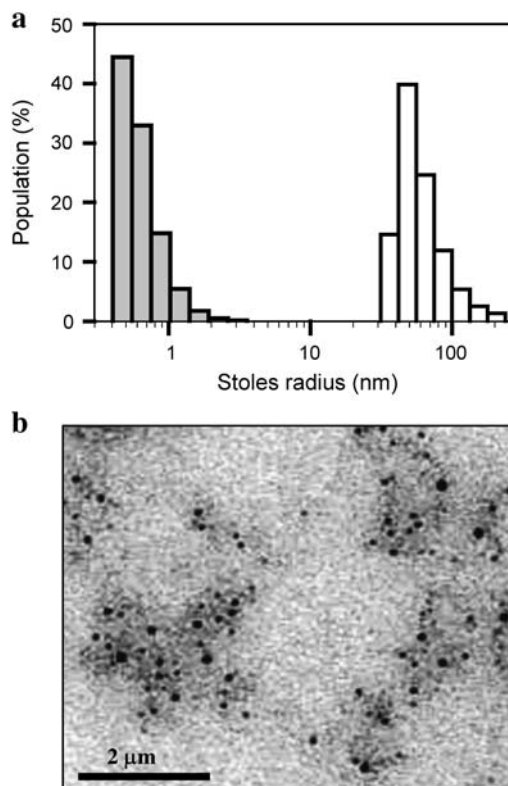
FIGURE 3 Size distribution of ThT-Ag nanoclusters. (*a*) Stokes radius of ThT-Ag nanoclusters generated in the aqueous solutions of ThT (10 μM)/ $AgNO_3$ (0.1 μM) and ThT (10 μM)/$AgNO_3$ (1 μM) as estimated by dynamic light scattering. The Stokes radius peaks are centered at 0.7 nm and 55.5 nm for the clusters generated in the solutions of ThT (10 μM)/$AgNO_3$ (0.1 μM) and ThT (10 μM)/$AgNO_3$ (1 μM), respectively. Both peaks have the same polydispersity of 41%. The error in the baseline of the autocorrelation function did not exceed 5%. (*b*) Electron micrograph of clusters generated in an aqueous solution of ThT (10 μM)/$AgNO_3$ (1 μM).

radii of 0.7 nm upon photoreduction of aqueous solutions of ThT (10 μM)/AgNO$_3$ (0.1 μM; Fig. 3 *a*). A 10-fold increase of AgNO$_3$ concentration in the presence of 10 μM ThT produced nanoclusters of substantially larger size (average Stokes radii = 55 nm). The nanoclusters generated in solutions of ThT (10 μM)/AgNO$_3$ (1 μM) were also visible by electron microscopy (Fig. 3 *b*).

We next sought to explore whether nanoclusters generated upon sensitized photoreduction can be detected using fluorescent microscopy. The aqueous solution of ThT (10 μM)/AgNO$_3$ (1 μM) showed numerous individual fluorescent clusters, which appeared only after 3 min of illumination (Fig. 1 *a*, *panel 2*). Each single cluster displayed time-dependent blinking (Fig. 1 *b*). The blinking dynamic was similar to that found for dendrimer-encapsulated silver nanodots (4). Analyses of the blinking dynamics of an individual cluster revealed an apparent on-time of $\tau_{on} = 55 \pm 5$ ms and an apparent off-time of $\tau_{off} = 470 \pm 50$ ms, where on-time is defined as the time width of a photon burst and off-time is the time between two consecutive photon bursts (Fig. 1 *c*). Such a dynamic is a characteristic of individual emitters and is typically found in single molecule fluorescence (18,19). We also noticed that the brightness of each individual cluster and the number of clusters located in the field of view increased during the first 10 min of observation. Instead of the photobleaching observed for organic fluorophores, hybrid nanoclusters showed additional photoactivation upon illumination at 475 nm. Our results demonstrated that hybrid nanoclusters are exceptionally bright and remarkably resistant to photobleaching and can be easily detected using a fluorescent microscope.

Next we explored whether hybrid organic-inorganic nanoclusters provided advantages in specific biological applications and, in particular, for imaging of amyloid fibrils. ThT is known to bind selectively to amyloid deposits and has been employed broadly to detect amyloid fibrils and plaques in vitro and in vivo (20). In the presence of amyloid fibrils, ThT displays a substantial change in excitation and emission spectra: a new excitation peak appears at 450 nm that was barely seen for the free dye (Fig. 2 *e*); the emission maximum of ThT shifts from 450 nm to above 480 nm (20). Therefore, in the presence of amyloid fibrils, we used new excitation wavelengths: at 458 nm for confocal microscopy and 475 nm for epifluorescence microscopy. The irradiation at 475 nm is not optimal, however, as it still overlaps substantially with the excitation spectra.

To test whether hybrid ThT-Ag nanoclusters retained the characteristic property of ThT to stain amyloid structures, we used recombinant human prion protein encompassing residues 90–231 (PrP 90–231) converted in vitro into the amyloid form (6). After incubation for 5 min with preformed ThT-Ag nanoclusters, amyloid deposits of PrP 90–230 were observed to be covered by blinking fluorescent clusters (Fig. 4 *a*, *panel 1*). The amyloid fibrils stained only with ThT showed rapid decay of fluorescence and were barely detectable after
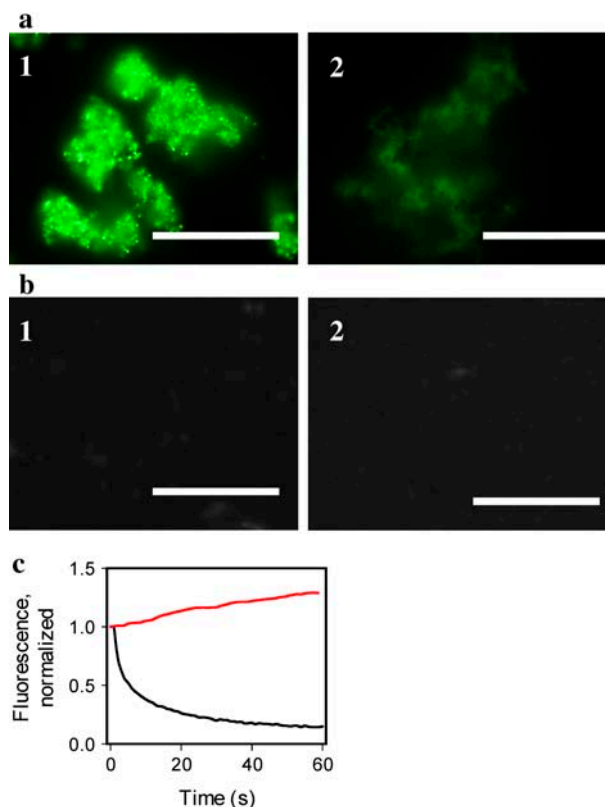

FIGURE 4 Staining of the amyloid fibrils with hybrid Ag-ThT nanoclusters. (*a*) Epifluorescence microscopy images of the amyloid fibrils of PrP 90–231 stained with preformed hybrid nanoclusters (*panel 1*, exposure time for collecting image is 0.02 s), and with 10 μM ThT (*panel 2*, exposure time 1.6 s), scale bars = 10 μm. Hybrid nanoclusters were generated by irradiation of aqueous solutions of ThT (10 μM)/AgNO$_3$ (1 μM) at 312 nm for 3 min. The amyloid fibrils were diluted to the final concentration of PrP 90–231 equivalent to 1 μM placed on a coverslip and incubated at room temperature in the presence of hybrid nanoclusters or ThT alone. (*b*) Epifluorescence microscopy of the nonamyloid β-oligomeric form of PrP 90–230 (*panel 1*, exposure time 1.6 s), and aggregated form of PrP 23–230 (*panel 2*, exposure time 1.6 s), stained with hybrid nanoclusters. Recombinant human PrP encompassing residues 90–231 was converted in vitro into the amyloid fibrils and the β-oligomeric form as described previously (6). The aggregated form of rPrP 23–230 was prepared as described by Zahn (21) and confirmed by size-exclusion chromatography and dynamic light scattering. (*c*) Photobleaching kinetics of the fibrils stained with ThT (*black line*) versus photoactivation kinetics of the fibrils stained with hybrid nanoclusters (*red line*). The kinetics of photobleaching/photoactivation was collected from a 5 μm × 5 μm area and normalized to the intensity measured at zero time.

one minute of illumination at 475 nm, despite an 80-fold longer exposure time (Fig. 4 *a*, *panel 2*). In contrast, amyloid aggregates stained with ThT-Ag nanoclusters displayed a time-dependent increase of fluorescence (Fig. 4 *c*). Remarkably, we did not notice any photobleaching effect even after 24 h of steady illumination at 475 nm at high irradiance (500 W/cm^2).

To test whether ThT-Ag nanoclusters preserve the specificity of binding to amyloid structures, we prepared two nonamyloid isoforms of the same protein, the α-helical

monomeric and the β-sheet rich oligomeric forms (6). No fluorescence was detected upon staining of either the α-helical monomer or β-oligomeric isoforms with hybrid nanoclusters using fluorescence microscopy (Fig. 4 b, panel 1). We also tested nonfibrillar aggregates of the full-length recombinant prion protein encompassing residues 23–231 (PrP 23–231). PrP 23–231 is known to form large non-amyloid aggregates upon incubation at room temperature at pH 7.0 in the presence of salt (21). These aggregates did not show detectible fluorescence despite an 80-fold longer exposure time (Fig. 4 b, panel 2).

Because each individual cluster displayed an unusually bright emission and was resistant to photobleaching, we next examined whether such properties were a result of metal-enhanced emission of ThT or an intrinsic fluorescent property of the silver of the nanoclusters. Silver is known to exhibit bright and photostable fluorescence as was previously shown for gaseous silver particles, silver deposited on surfaces, and silver dots encapsulated into dendrimers, but not for silver in aqueous solutions (3,4,22,23). To address this question we compared the emission spectra collected from an area of view densely populated with nanoclusters to spectra recorded from the fibrils prestained only with ThT. Emission spectra of
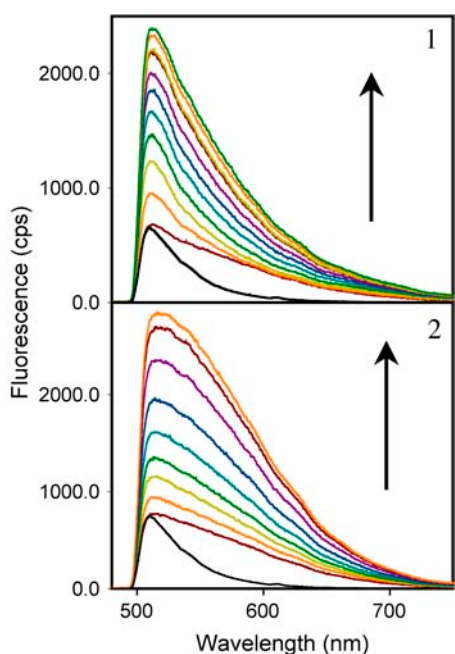

FIGURE 5 Bulk emission spectra of the amyloid fibrils stained with hybrid nanoclusters. The emission spectra of fibrils stained with the hybrid nanoclusters generated in ThT (10 μM)/AgNO$_3$ (0.1 μM; colored lines, panel 1) and ThT (10 μM)/AgNO$_3$ (1 μM; colored lines, panel 2). Hybrid nanoclusters display time-dependent increase of emission intensity during the first 10 min of observation as shown by arrows (from the bottommost spectra to the topmost spectra). Bulk emission spectra of fibrils stained with ThT alone are shown for comparison (black lines); ThT spectra were normalized relative to the bottommost spectrum of hybrid nanoclusters. All spectra were recorded upon excitation at 475 nm (irradiance 500 W/cm^2) using a 510 nm long-path filter.

blinking nanoclusters were notably different from those of ThT (Fig. 5). In comparison to the emission of ThT, the spectra of nanoclusters generated in solutions of ThT (10 μM)/AgNO$_3$ (0.1 μM) were characterized by a larger half-width and by a red-shift of the emission maximum (Fig. 5, panel 1). The nanoclusters generated at higher concentrations of AgNO$_3$ (1 μM) displayed an even larger half-width of the emission maximum due to an additional increment of fluorescence emission at longer wavelengths (Fig. 5, panel 2).

At each particular molar ratio of AgNO$_3$ to ThT, the emission intensity increased gradually upon permanent illumination at 475 nm, whereas the shape of spectra did not change substantially over the time course of illumination. However, when the molar ratio of AgNO$_3$ to ThT increased from 0.01 to 0.1, the emission spectra showed characteristic changes (Fig. 5, compare panels 1 and 2). The time-dependent growth of the emission intensity upon illumination at 475 nm can be explained by the increase in number of clusters and/or brightness of individual clusters rather than by the change in cluster composition. The red-shift in emission spectra observed at concentrations of AgNO$_3$ higher than 0.1 μM, however, was indicative of a change in cluster composition and is consistent with the incorporation of larger amounts of silver into nanoclusters. As judged from the spectral properties and blinking dynamics, the emission of hybrid nanoclusters resembled the fluorescence observed from dendrimer-encapsulated silver nanodots (4). Taken together our data indicate that, besides metal-enhanced fluorescence of ThT, under illumination with high irradiance produced by the metal halide lamp of the fluorescent microscope (500 W/cm^2), hybrid clusters also produced an extra bright blinking emission typical for the intrinsic fluorescence of silver.

Our previous experiments demonstrated the possibility that photoinduced generation of nanoclusters might occur not only upon UV irradiation but also upon illumination with visible light up to 500 nm. Therefore we set out to determine whether hybrid nanoclusters could be formed in situ, e.g., on amyloid fibrils prestained with ThT. Since efficient photoinduced reduction of Ag$^+$ requires ThT, we expected that the hybrid nanoclusters would appear at loci with high concentrations of ThT. Amyloid fibrils were prestained with ThT (10 μM), treated with AgNO$_3$ directly on a coverslip in the presence of ThT, and observed microscopically upon illumination at 475 nm. The fibrils treated with the lowest concentration of AgNO$_3$ (0.1 μM) showed time-dependent increases of fluorescent intensity (Fig. 6 a, panels 1 and 2). However, no individual clusters were clearly detectable. Increasing AgNO$_3$ concentration 10-fold to 1 μM resulted in formation of multiple fluorescent nanoclusters on amyloid aggregates (Fig. 6 a, panel 3). Upon continuous illumination at 475 nm in the presence of ThT and AgNO$_3$, the number of fluorescent clusters as well as the brightness of each individual cluster increased. Analysis of the blinking dynamics demonstrates that the brightness of individual clusters increased due to overall growth of blinking amplitude (Fig. 6
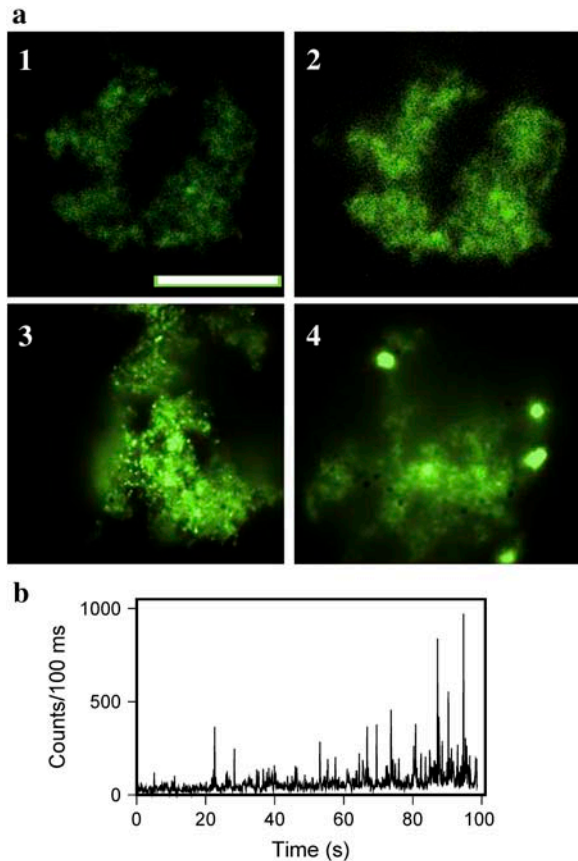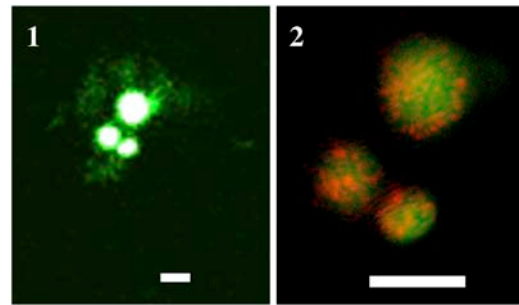
FIGURE 6 Generation of hybrid nanoclusters in situ. (*a*) Epifluorescence microscopy images of amyloid fibrils prestained with ThT (10 μM) followed by in situ photoreduction with different concentrations of AgNO$_3$: 0.1 μM at time zero (*panel 1*) and after 2 min of irradiation at 475 nm (*panel 2*), 1 μM AgNO$_3$ after 2 min of irradiation (*panel 3*), and 10 μM AgNO$_3$ after 2 min of irradiation (*panel 4*); scale bar = 10 μm. Exposure time for collecting images was 0.08 s for panels 1 and 2 and 0.02 s for panels 3 and 4. (*b*) Emission blinking observed from randomly selected single Ag-ThT nanoclusters monitored during formation of nanoclusters in situ. Emission was acquired for 1000 frames with 100-ms time resolution for each frame. Fluorescence was recorded with an irradiance of 500 W/cm^2.

FIGURE 7 Laser scanning confocal microscopy images of large clusters. Images were obtained by acquisition of emission at 510 nm upon excitation at 458 nm without zoom (*panel 1*) and with zoom and acquisition on two channels: green, emission at 510 nm upon excitation at 458 nm; and red, reflectance mode (*panel 2*); scale bars = 1 μm. Clusters were generated in situ upon incubation of amyloid fibrils of PrP 90–231 (1 μM) with ThT (10 μM) and AgNO$_3$ (10 μM) and illumination at 450 nm with an irradiance of 500 W/cm^2 for 5 min.

b). Appearance of bright individual clusters in situ upon increase of AgNO$_3$ concentration was consistent with our early observation of the increase in cluster size as judged from dynamic light scattering (Fig. 3 *a*). At the highest concentration of AgNO$_3$ (10 μM) tested, few large extra bright clusters were observed (Fig. 6 *a*, *panel 4*). The nanoclusters generated in situ displayed photostable fluorescence even after removal of free silver and ThT from solution by rinsing.

To investigate the structure of the large clusters, we employed confocal microscopy with simultaneous acquisition of fluorescence images collected at 510 nm and reflected light images recorded in the laser reflection mode at 458 nm (Fig. 7 *b*). Dual imaging revealed the fine substructure within the hybrid clusters where subclusters of silver were distributed along the cross sections of clusters as seen in the laser reflection mode (Fig. 7 *b*, *panel 2*). This result con-

firmed that hybrid nanoclusters are composed of ThT and silver.

To gain additional insight into the mechanism of cluster formation, we tested whether generating nanoclusters in situ requires the presence of both ThT and silver at the same time during photoactivation. When fibrils were pretreated with ThT (10 μM) then rinsed to remove free ThT from solution and subsequently incubated with AgNO$_3$ (1 μM), no nanoclusters were detected upon illumination at 475 nm. Vice versa, when the fibrils were first pretreated with AgNO$_3$ (1 μM), illuminated, washed from free AgNO$_3$, and then incubated with ThT (10 μM), no nanoclusters were seen upon illumination at 475 nm. These experiments indicated that the presence of both free ThT and silver in solution during photoactivation is required for generating nanoclusters. Interestingly, when fibrils were first pretreated with AgNO$_3$ and then with ThT in the absence of AgNO$_3$, ThT fluorescence observed from such fibrils appeared to be more photostable over time than the fluorescence observed from the fibrils that were not pretreated with AgNO$_3$. One may speculate that fibrils pretreated with AgNO$_3$ bind residual amounts of silver that can stabilize ThT-fluorescence. However, the amount of silver bound to fibrils may not be sufficient for generating nanoclusters.

Next we thought to test whether in situ photoreduction can be applied for imaging a single fibril. For this purpose we used recombinant mouse full-length PrP 23–231, as it forms long fibrils in vitro (Fig. 8, *panel 1*; (7)). Upon staining with ThT followed by in situ photoreduction in the presence of a low concentration of AgNO$_3$ (0.1 μM), we observed an alternating pattern of relatively bright and dim emissions distributed along the *z* axis of each fibril (Fig. 8, *panel 2*). When AgNO$_3$ concentration was increased to 1 μM, a regular pattern of extra bright fluorescent nanoclusters appeared along each fibril (Fig. 8, *panel 3*). Because the growth of fluorescent clusters is stimulated by high local concen-
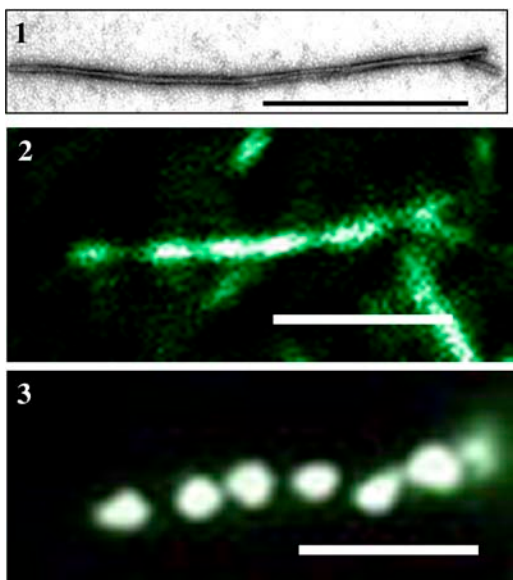
FIGURE 8 Imaging of single amyloid fibrils. The single fibril of recombinant mouse full-length PrP 23–231 viewed by electron microscopy (*panel 1*), by epifluorescent microscopy after prestaining with ThT (10 μM) followed by in situ photoreduction with 0.1 μM AgNO$_3$ (*panel 2*), and with 1 μM AgNO$_3$ (*panel 3*). Scale bars = 1 μm.
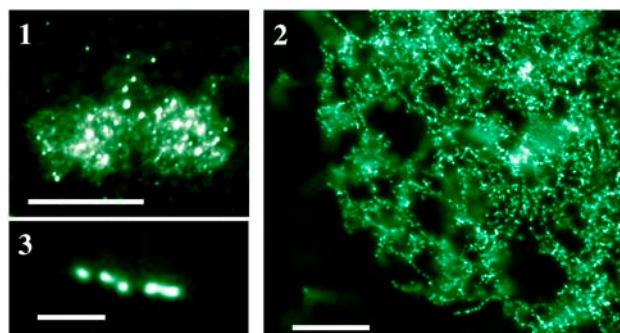

FIGURE 9 Imaging of amyloid fibrils of insulin. Epifluorescence microscopy images of fibrils aggregated in solution (*panel 1*), fibrils sedimented on the surface of a coverslip (*panel 2*), and an image of a single fibril (*panel 3*). Amyloid fibrils produced from bovine insulin were prestained with ThT (10 μM) then treated with AgNO$_3$ (10 μM) directly on a coverslip in the presence of ThT and observed microscopically upon illumination at 475 nm. Scale bars are 5 μm (*panels 1* and *2*) and 1 μm (*panel 3*).

trations of ThT, one can speculate that the periodicity of clusters reflected regularities in fibrillar morphology. This result demonstrates that sensitized photoreduction in situ can be used for detection and imaging of single amyloid fibrils in aqueous solution. Because the spatial resolution of the fluorescent imaging is limited by diffraction, the extent to which this method will be useful for examining the substructure of single fibrils has yet to be determined.

To test whether the ability to generate ThT-Ag nanoclusters is limited to fibrils of prion proteins or not, we prepared amyloid fibrils from insulin and lysozyme. Both proteins are known to be amyloidogenic and can be converted into the fibrillar form upon incubating at acidic pH and elevated temperatures (8,9). We found that a substantial subfraction of fibrils produced from insulin aggregated into large clumps and remained in solution, and some fibrils sedimented onto the glass surface of a coverslip. Upon incubation with ThT and AgNO$_3$ followed by irradiation at 475 nm, both types of fibrillar aggregates, the ones found in solution and on the surface, generated bright nanoclusters (Fig. 9, *panels 1* and *2*, respectively). A regular pattern of extra bright fluorescent nanoclusters can be seen along a single fibril of insulin (Fig. 9, *panel 3*), similar to that observed for fibrils of full-length PrP. Amyloid fibrils generated from lysozyme also produced fluorescent nanoclusters (data not shown). These data demonstrate that the ability to form ThT-Ag nanoclusters is not restricted to fibrils of mammalian prion proteins but rather is a generic feature of amyloid conformation.

DISCUSSION

Several recent studies described the phenomenon of metal-enhanced fluorescence of organic fluorophores (24). To date, this phenomenon has been confined to silver island films and silver colloids, where the deposition of organic fluorophores on the metallic structures resulted in substantial increases of the quantum yield (25). Here we present the first example, to our knowledge, of water-soluble hybrid Ag-ThT nanoclusters that exhibit metal-enhanced fluorescence. In our experience, once generated, hybrid nanoclusters remained water soluble for at least 3 months and displayed a very bright and photostable emission.

The molecular mechanism responsible for the enhancement of ThT/Ag emission that accompanies sensitized photoreduction remains unclear at this point. Hybrid nanoclusters exhibit a unique combination of fluorescence properties. At high excitation intensity (irradiance ~500 W/cm^2), which we employed for our fluorescence microscopy studies, they display extra bright blinking silver fluorescence. As judged from the emission spectra the silver fluorescence, together with the metal-enhanced fluorescence of the organic dye ThT, contributed to the total emission enhancement (Fig. 5). However, at low excitation intensity (irradiance ~1 W/cm^2), which was used for measuring spectra in bulk solutions, the emission spectra were similar to those of ThT alone and can be predominantly attributed to the metal-enhanced intrinsic fluorescence of ThT. One can propose that the enhancement of ThT fluorescence is due to the aggregation-induced planarization of ThT (26). Upon coaggregation with Ag^0, ThT molecules may convert from a twisted conformation in which the emission is suppressed to the coplanar one, which is characterized by efficient emission. Besides an intramolecular effect, the enhancement of fluorescence may also be due to an intermolecular effect, i.e., formation of J-type aggregates, where ThT molecules are arranged in a head-to-

tail direction (26,27). With respect to the intrinsic fluorescence of silver, it is known that water is one of the factors that can quench the fluorescence of Ag nanoclusters (28). It is likely that the fluorescence quantum efficiency of Ag will benefit from formation of hybrid clusters with ThT, which may protect Ag from interacting with water. Nonetheless, regardless of the mechanism responsible for the enhanced fluorescence of ThT and Ag, the rare combination of photostability and high brightness should be beneficial for imaging low-abundant targets and for the development of ultrasensitive biological assays.

To test whether other compounds can be used instead of ThT for generating hybrid nanoclusters, we tested several classes of fluorescent compounds including carbocyanines, rhodamine, ethidium bromide, and primulin. We were unable to produce fluorescent clusters using the aforementioned compounds. Therefore, the property of ThT in accelerating formation of hybrid nanoclusters seems to be quite unique. From one perspective, this fact may limit the applicability of this method for biological imaging. On the other hand, the inability of silver to form hybrid nanoclusters with other organic dyes may provide certain advantages for those applications where silver-ThT nanoclusters need be used in combination with other fluorophores for double staining. Lack of cross-reactivity between silver and other organic fluorophores excludes potential artifacts related to the formation of hybrid nanoclusters between silver and non-ThT dyes. At the same time, the possibility that some other dyes or derivatives of ThT would be able to generate hybrid nanoclusters cannot be fully excluded and needs to be tested in future studies. Noble metals are known to form nanocomposites with diverse classes of organic compounds including fluorescent dyes (1). However, whether the emission properties of any other organic dyes can be improved by incorporating into hybrid organic-inorganic nanocomposites remains to be established.

Our findings demonstrate that sensitized photoreduction of Ag^+ in aqueous solutions produces a novel class of nanoclusters with a unique combination of fluorescent properties. The efficiency of generating fluorescent nanoclusters by sensitized photoreduction of Ag^+ is at least 100-fold higher than that reported for direct photoactivation (4,29). Since the hybrid nanoclusters are water soluble and extremely resistant to photobleaching, they offer exceptional advantages over organic fluorophores for detection of low abundance targets in vitro and in vivo.

An alternative procedure for generating fluorescent silver nanocomposites was described recently by Zheng and Dickson (4). Their procedure involves encapsulation of Ag nanodots into dendrimers followed by photoactivation with blue light (450–480 nm). The size of the dendrimer encapsulated nanodots is usually smaller than that of the silver-ThT nanoclusters described here, and it is limited by the size of the dendrimer that can be synthesized (4.5 nm and 3 nm in diameter for fourth- and second-generation, respectively). In contrast to the dendrimer encapsulated nanodots, the size of silver-ThT nanoclusters is not limited; therefore, the brightness of nanoclusters can be increased by increasing the cluster's size. Another advantage of hybrid clusters prepared by sensitized photoreduction with ThT is the ability to generate fluorescent probes in situ. The process of sensitized photoreduction of Ag^+ allows for the turning on of the fluorescent probes in a time- and space-dependent manner. As the concentrations of silver required to generate hybrid nanoclusters are below cytotoxic concentrations found for prolonged exposures of cells to Ag^+ (30), one may speculate that hybrid nanoclusters can be applicable for long-term tracking of biological processes and for detecting low-abundant targets in living cells. Whether or not hybrid nanoclusters or byproducts of photoactivation are toxic to cells remains to be addressed in future studies. As the size and the emission intensity of hybrid clusters are regulated by the concentration of Ag^+, the sensitivity of detection can be considerably enhanced. Therefore, the range of practical biological applications can be expanded to the development of ultrasensitive biological assays.

REFERENCES

1. Kamat, P. V. 2002. Photophysical, photochemical and photocatalytic aspects of metal nanoparticles. *J. Phys. Chem.B*. 106:7729–7744.

2. Konig, L., I. Rabin, W. Schulze, and G. Ertl. 1996. Chemiluminescence in the agglomeration of metal clusters. *Science*. 274:1353–1355.

3. Geddes, C. D., A. Parfenov, I. Gryczynski, and J. R. Lakowicz. 2003. Luminescent blinking from silver nanostructures. *J. Phys. Chem. B*. 107:9989–9993.

4. Zheng, J., and R. M. Dickson. 2002. Individual water-soluble dendrimer-encapsulated silver nanodot fluorescence. *J. Am. Chem. Soc*. 124:13982–13983.

5. Petty, J. T., J. Zheng, N. V. Hud, and R. M. Dickson. 2004. DNA-templating Ag nanocluster formation. *J. Am. Chem. Soc*. 126:5207–5212.

6. Baskakov, I. V. 2004. Autocatalytic conversion of recombinant prion proteins displays a species barrier. *J. Biol. Chem*. 279:586–595.

7. Bocharova, O. V., L. Breydo, A. S. Parfenov, V. V. Salnikov, and I. V. Baskakov. 2005. In vitro conversion of full length mammalian prion protein produces amyloid form with physical property of PrPSc. *J. Mol. Biol*. 346:645–659.

8. Krebs, M. R. H., C. E. MacPhee, A. F. Miller, I. E. Dunlop, C. M. Dobson, and A. M. Donald. 2004. The formation of spherulites by amyloid fibrils of bovine insulin. *Proc. Natl. Acad. Sci. USA*. 101:14420–14424.

9. Frare, E., P. P. deLaureto, J. Zurdo, C. M. Dobson, and A. Fontana. 2004. A highly amyloidogenic region of hen lysozyme. *J. Mol. Biol*. 340:1153–1165.

10. Hada, H., Y. Yonezawa, A. Yoshida, and A. Kurakake. 1976. Photoreduction of silver ion in aqueous and alcoholic solutions. *J. Phys. Chem*. 80:2728–2731.

11. Henglein, A., P. Mulvaney, and T. Linnert. 1991. Chemistry of silver aggregates in aqueous solution: non-metallic oligomers and metallic particles. *Electrochim. Acta.* 36:1735–1741.

12. Sato, T., H. Onaka, and Y. Yonezawa. 1999. Sensitized photoreduction of silver ions in the presence of acetophenone. *J. Photochem. Photobiol. A: Chem.* 127:83–87.

13. Lakowicz, J. R. 1999. Principles of Fluorescence Spectroscopy. Kluwer Academic/Plenum Publishers, New York.

14. Tong, M. L., X. L. Yu, and X. M. Chen. 2000. Synthesis and structure of a photoluminescent three-dimensional network [AgL(MeCN)] (L=4,5-dichloro-2-cyano-3,6-dione-1,4-cyclohexen-1-ol anion). *Inorg. Chem. Commun.* 3:694–696.

15. Zheng, J., J. Petty, and R. M. Dickson. 2003. High quantum yield blue emission from water-soluble Au8 nanodots. *J. Am. Chem. Soc.* 125:7780–7781.

16. Balogh, L., D. R. Swanson, D. A. Tomalia, G. L. Hagnauer, and A. T. McManus. 2001. Dendrimer-silver complexes and nanocomposites as antimicrobial agents. *Nano Lett.* 1:18–21.

17. Esumi, K., A. Suzuki, A. Yamahira, and K. Torigoe. 2000. Role of poly(amidoamine) dendrimers for preparing nanoparticles of gold, platinum, and silver. *Langmuir.* 16:2604–2608.

18. Dickson, R. M., A. B. Cubitt, R. Y. Tsien, and W. E. Moerner. 1997. On/Off blinking and switching behaviour of single molecules of green fluorescent proteins. *Nature.* 388:355–358.

19. Garcia-Parajo, M. F., G. M. J. Segers-Nolten, J.-A. Veerman, J. Greve, and N. F. van Hulst. 2000. Real-time light-driven dynamics of the fluorescence emission in single green fluorescent protein molecules. *Proc. Natl. Acad. Sci. USA.* 97:7237–7242.

20. LeVine, H. 1993. Thioflavine T interaction with synthetic Alzheimer's disease β-amyloid peptides: detection of amyloid aggregation in solution. *Protein Sci.* 2:404–410.

21. Zahn, R. 2003. The octapeptide repeats in mammalian prion protein constitute a pH-dependent folding and aggregation site. *J. Mol. Biol.* 334:477–488.

22. Ievlev, D., I. Rabin, W. Schulze, and G. Ertl. 2000. Light emission in the agglomeration of silver clusters. *Chem. Phys. Lett.* 328:142–146.

23. Maali, A., T. Cardinal, and M. Treguer-Delapierre. 2003. Intrinsic fluorescence from individual silver nanoparticles. *Physica E.* 17:559–560.

24. Kummerlen, J., A. Leitner, H. Brunner, F. R. Aussenegg, and A. Wokaun. 1993. Enhanced dye fluorescence over silver island films: analysis of the distance dependence. *Mol. Phys.* 80:1031–1046.

25. Parfenov, A., I. Gryczynski, J. Malicka, C. D. Geddes, and J. R. Lakowicz. 2003. Enhanced fluorescence from fluorophores on fractal silver surfaces. *J. Phys. Chem. B.* 107:8829–8833.

26. An, B. K., S. K. Kwon, S. D. Jung, and S. Y. Park. 2002. Enhanced emission and its switching in fluorescent organic nanoparticles. *J. Am. Chem. Soc.* 124:14410–14415.

27. Xiao, D., L. Xi, W. Yang, H. Fu, Z. Shuai, Y. Fang, and J. Yao. 2003. Size-Tunable emission from 1,3-Diphenyl-5-(2-anthryl)-2-pyrazoline nanoparticles. *J. Am. Chem. Soc.* 125:6740–6745.

28. Mihalcea, C., D. Buchel, N. Atoda, and J. Tominaga. 2001. Intrinsic fluorescence and quenching effects in photoactivated reactively sputtered silver oxide layers. *J. Am. Chem. Soc.* 123:7172–7173.

29. Peyser, L. A., A. E. Vinson, A. P. Bartko, and R. M. Dickson. 2001. Photoactivated fluorescence from individual silver nanoclusters. *Science.* 291:103–106.

30. Wataha, J. C., P. E. Lockwood, and A. Schedle. 2000. Effect of silver, copper, mercury, and nickel ions on cellular proliferation during extended, low-dose exposures. *J. Biomed. Mater. Res.* 52:360–364.

31. LeVine, H. 1999. Quantification of beta-sheet amyloid fibril structure with thioflavin T. *Methods Enzymol.* 309:274–284.